Journal of the Optical Society of America B
OPTICAL PHYSICS

# Mid-infrared supercontinuum generation in $As_2S_3$-circular photonic crystal fibers pumped by 4.5 μm and 6 μm femtosecond lasers

Ben Chu Van,[1] Bao Tran Le Tran,[2] and Lanh Chu Van[2,*]

[1]Faculty of Electronic Engineering I, Posts and Telecommunications Institute of Technology, Hanoi, Vietnam
[2]Department of Physics, Vinh University, Vinh City, Nghe An Province, Vietnam
*chuvanlanh@vinhuni.edu.vn

Received 2 July 2024; accepted 5 July 2024; posted 9 July 2024; published 5 August 2024

**A study on $As_2S_3$ chalcogenide photonic crystal fiber (PCF) and its potential in supercontinuum generation (SCG) applications is presented. The designed fibers exhibit near-zero flattened chromatic dispersion, facilitating coherent and broad SCG utilizing femtosecond lasers at 4.5 and 6 μm wavelengths. A continuous spectrum spanning from 1.5 to 8 μm is achieved when the initial fiber is stimulated with an input power of 20 kW. With a pulse width of 100 fs and input power of 6 kW, the second fiber provides soliton-induced SCG with 2 to 15 μm spectral bandwidth. Furthermore, the integration of these large core diameter PCFs with high-power laser pulses guarantees the preservation of optical fiber integrity without damage. Consequently, these fibers hold promise for delivering SC spectra characterized by high power density, catering to a diverse range of practical applications including optical communications, spectroscopy, sensing, metrology, and calibration.** 

https://doi.org/10.1364/JOSAB.534504

## 1. INTRODUCTION

In recent years, there has been a global focus on mid-infrared (MIR) laser sources due to their wide-ranging applications in biomedical science [1], materials processing [2], and molecular spectroscopy [3]. The interest in ultra-broadband MIR supercontinuum sources is driven by the vibrational resonances of molecules in this range [2,3]. To efficiently generate a MIR supercontinuum, it is essential to combine an ultrafast laser with a highly nonlinear waveguide. Fiber-based pump sources, specifically all-fiber SC sources, are preferred over chip-based schemes due to their ability to handle high power and offer superior quality [4–8]. Notably, there have been significant advancements in MIR fiber lasers with pulse durations as short as several cycles, such as femtosecond lasers with wavelengths of 4.5 μm and 6 μm [9–11]. These are anticipated to serve as the pump source for MIR supercontinuum generation.

The utilization of silica glass photonic crystal fiber (PCF) with a solid core in the process of SCG across various spectral regions such as UV, visible, and near-infrared (NIR) has garnered significant interest [12]. However, its effectiveness in the mid-infrared (MIR) region is constrained due to the high loss of silica at wavelengths exceeding 2.4 μm [12]. Therefore, there is a need to explore alternative non-silica-based fibers to enhance SCG in the infrared wavelength range. In recent developments, transparent organic solvents within the visible-IR ranges have been employed to fill the hollow core of the PCF [13–15]. It is worth noting that the nonlinear refractive index of these organic solvents surpasses that of silica, potentially enabling liquid PCFs to facilitate SCG across a wider bandwidth with low peak power requirements. However, challenges persist in effectively transporting the liquid to the end of the fiber without leakage, as well as in stabilizing the output spectrum of PCFs over extended durations [16,17].

The transparency of soft glass-based PCFs surpasses the multi-phonon absorption region of fused silica, particularly for chalcogenide glasses with a transparency range of up to 25 μm. Additionally, these glasses exhibit extremely high nonlinearities. However, devices based on chalcogenide suffer from low stability due to the susceptibility of materials to degradation and mechanical fragility [18]. Various types of chalcogenide fibers have been developed, such as GeAsTeSe, GeAsSe, Te-As-Se, AsSe, and AsS [19–23]. To address these challenges, a pressure-assisted melt-filling technique utilizing an $As_2S_3$ waveguide has been introduced, resulting in the generation of octave-spanning mid-infrared supercontinuum generation with high coherence [22,24]. Similar to other chalcogenides, $As_2S_3$ offers a broad transmission window from visible to mid-infrared spectral ranges, enabling efficient light confinement and significant nonlinearity. The popularity of $As_2S_3$ PCFs in scientific applications is evident through theoretical and experimental works in optical and photonic domains over the years [23–28].

This study demonstrates the SCG in $As_2S_3$ circular PCFs with low loss and broad bandwidth using 4.5 μm and 6 μm femtosecond lasers as pump sources. The research explores the nonlinear dynamics of SCG in different dispersion regimes. Additionally, a novel $As_2S_3$ circular PCF with seven air-hole rings is designed and analyzed, showcasing wide spectra and high coherence. The benefits of using a circular lattice for broadband SCG, such as longer dispersion lengths and increased soliton interaction, have also been demonstrated previously [29].

## 2. PCF DESIGN AND CHROMATIC DISPERSION CHARACTERISTIC

Figure 1 depicts the designed solid-core PCF model surrounded by seven additional rings. $As_2S_3$ is chosen as the background material owing to its good transmission in the MIR and other benefits described in Section 1. Its nonlinear refractive index is $42 \times 10^{-19}$ $m^2/W$, which is 153 times higher than that of silica. The refractive index of $As_2S_3$ and its Sellmeier coefficients is shown in the Fig. 2. The real fraction of the refractive index of $As_2S_3$ can be determined by the Sellmeier relationship because the refractive index depends on wavelength [Eq. (1)] [22],

$$n(\lambda) = \sqrt{1 + \sum \frac{X_i \lambda^2}{\lambda^2 - Y_i^2}}, \tag{1}$$

where λ is the operating wavelength in free space, and $X_i$ and $Y_i^2$ $(i = 1, 2, 3)$ are the Sellmeier coefficient of the material.

All cladding holes are assumed to have the same diameter ($d$) to facilitate future fiber fabrication. Another geometric parameter of PCF is the lattice pitch (Λ). Note that the value of the air hole diameter to pitch factor ($f = d/\Lambda$) can be modified within the drawing process by adjusting the gas pressure inside the cladding [30]. A larger $f$ requires higher gas pressure, which can result in unevenly created air holes. Conversely, using a small $f$ leads to a large effective mode area and high loss, which reduces the nonlinear coefficients necessary for spectrum broadening. Therefore, in numerical simulations, we vary the $f$ from 0.3 to 0.6 with a 0.1 step for lattice pitches of 2.0 μm, 2.5 μm, and 3.0 μm, respectively. The core diameter in the designed fiber ($D_c = 4\Lambda - d$) ensures efficient coupling between this PCF and standard silica fibers. In a publication [31], Trong *et al.* studied the dispersion characteristics of square PCF with an

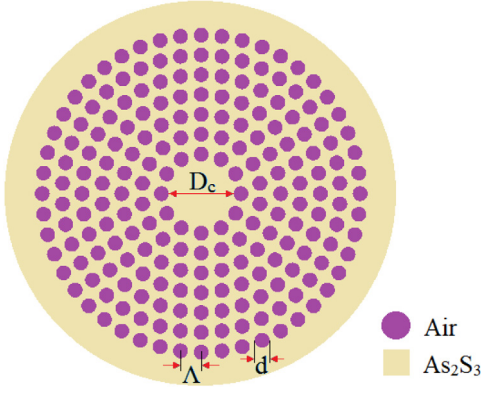


**Fig. 1.** Geometrical structure of PCF based on $As_2S_3$ with circular lattice.

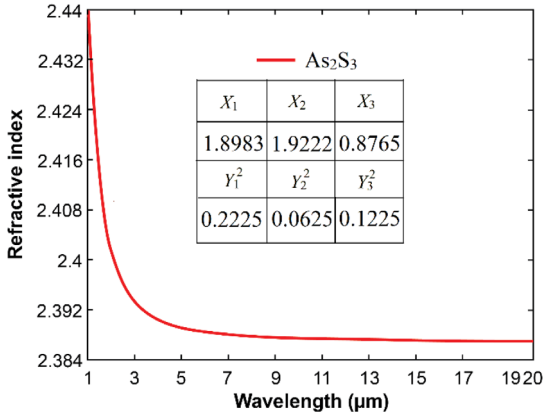


**Fig. 2.** Refractive index of $As_2S_3$ and its Sellmeier properties (in the inserted table).

$As_2S_3$ substrate. While PCFs with small core diameters significantly enhance the Kerr nonlinear coefficient, they also cause large losses at long wavelengths, limiting spectral broadening. Additionally, this work has not applied the optimal results of dispersion for SC generation. With a suitable structure, our PCFs contribute to achieving a shift to shorter wavelengths of zero-dispersion wavelength (ZDW) and near-zero dispersion curves for SCG. The full-vectorial finite element method combined with commercial Mode Solutions software is applied for dispersion calculations.

Designing PCFs with large cores can affect the effective refractive index of the core and cladding, i.e., the waveguide dispersion varies with wavelength. This means that the dispersion characteristic of $As_2S_3$ PCF can be flexibly controlled in a certain wavelength region, as shown in Fig. 3. It can be observed that fibers with smaller lattice pitches are less likely to support conduction mode within the core at long wavelengths. That is the reason why the simulation data are only shown at maximum wavelengths of 11 μm and 14 μm for fibers with $\Lambda = 2.0$ μm and 2.5 μm, respectively. Otherwise, structures with $\Lambda = 3.0$ μm can confine light in a wide wavelength range up to 17 μm. Additionally, while the dispersion curves tend to be red-shifted, their profiles change insignificantly as Λ increases. Initially, when $f = 0.3$, an all-normal dispersion profile is only achieved with the fiber with $\Lambda = 2.0$ μm, which is shown in Fig. 3(a) and the inset. When the pitch factor is larger than 0.3 [Figs. 3(b)–3(d)], all anomalous dispersion curves exhibit two ZDWs. At this point, decreasing the lattice pitch results in a blue shift of the ZDW. Modification of the structural parameters changes the flatness and slope of dispersion curves. A flat dispersion profile with two ZDWs, which is significant for broad SCG, is achieved with fiber having $\Lambda = 3.0$ μm and $f = 0.3$ due to its small dispersion value. Its flat dispersion range is between 4.42 μm and 7.69 μm with a value of 5 ps/nm/km (approximately 0.5 ps/nm/km variation).

To achieve various flattened chromatic dispersion profiles for different applications, it is necessary to optimize structural parameters such as $D_c$, $f$, and Λ. Based on preliminary analysis, the fiber with $f = 0.3$ ($\Lambda = 2.0$ μm) is chosen for SCG in an all-normal dispersion regime, while the fiber with $f = 0.3$ ($\Lambda = 3.0$ μm) is selected for SCG in anomalous dispersion one, denoted as $F_1$ and $F_2$, respectively. Although SCG with

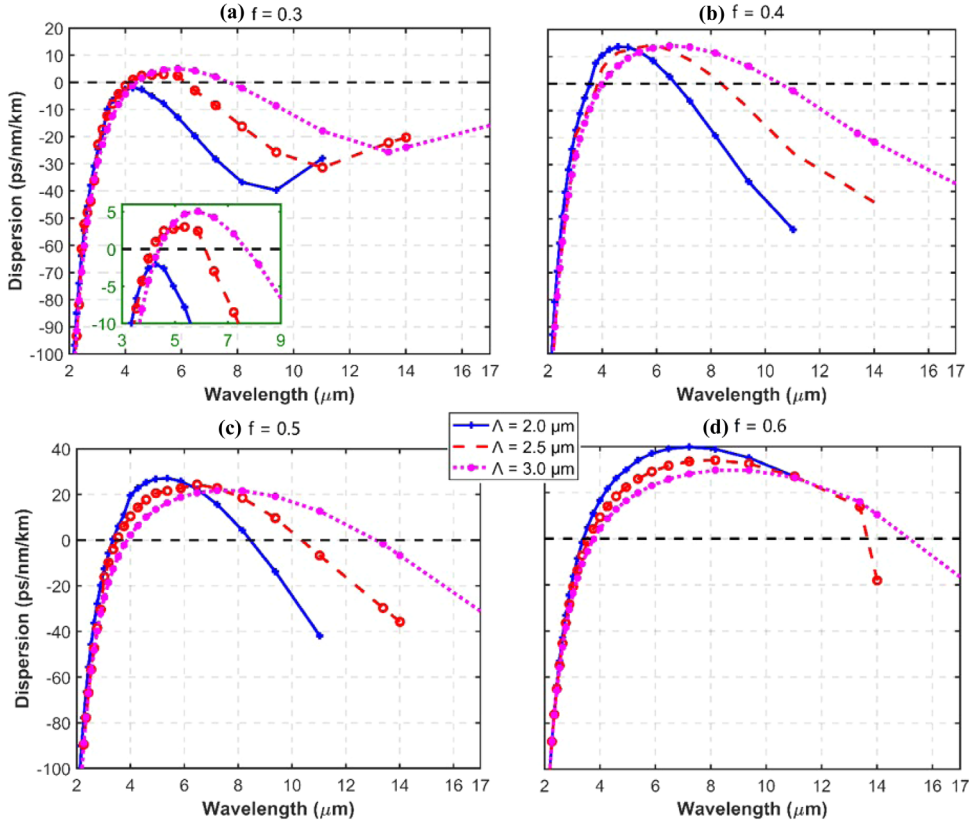


**Fig. 3.** Dispersion characteristics of the $As_2S_3$-based PCFs for (a) $f = 0.3$, (b) $f = 0.4$, (c) $f = 0.5$, (d) $f = 0.6$ and different lattice pitches.

**Table 1. Flattened Dispersion Range of the Proposed Fibers Compared with Previous Publications**

| Ref. | Regime | $f$ | Λ (μm) | Maximum Dispersion (ps/nm/km) | Flattened Dispersion Range (μm) |
|---|---|---|---|---|---|
| [31] | All-normal | 0.3 | 3.0 | $-9.736 \pm 0.5$ | 3.21–4.29 |
| [32] | All-normal | 0.4 | 2.5 | $-4.1 \pm 0.5$ | 3.66–4.44 |
| [33] | All-normal | 0.35 | 1.5 | $-3.74 \pm 1$ | 4.12–5.57 |
| [33] | All-normal | 0.3 | 1.5 | $-10.325 \pm 0.5$ | 4.22–5.96 |
| [33] | All-normal | 0.35 | 1.5 | $-0.92 \pm 0.5$ | 4.05–5.35 |
| **This work, $F_1$** | **All-normal** | **0.3** | **2.0** | $\mathbf{-2.01 \pm 0.5}$ | **3.96–5.46** |
| [22] | Anomalous | 0.35 | 2.0 | $11.65 \pm 1$ | 5.18–7.01 |
| [30] | Anomalous | 0.7 | 4.0 | $14.19 \pm 1$ | 2.59–3.63 |
| [31] | Anomalous | 0.35 | 3.0 | $2.26 \pm 0.5$ | 3.5–4.28 |
| [32] | Anomalous | 0.65 | 1.0 | $1.29 \pm 0.5$ | 2.32–2.41 |
| **This work, $F_2$** | **Anomalous** | **0.3** | **3.0** | $\mathbf{5.04 \pm 0.5}$ | **4.42–7.69** |

anomalous dispersion may be supported by smaller core structures, its flat band is limited. To emphasize the superiority of the selected fibers, an investigation of the flat dispersion band is conducted and compared with previous work in Table 1. For example, when $f = 0.3$ and $\Lambda = 1.5$ μm, a flat all-normal dispersion profile within the narrow wavelength range of 4.22–5.96 μm with a highest value of −10.325 ps/km/nm is reported by Thuy *et al*. [33]. Additionally, Lanh *et al*. discovered an anomalous chromatic dispersion curve with a flattened region of $11.65 \pm 1$ ps/km/nm between 5.18 and 7.01 μm when $f = 0.35$ and $\Lambda = 2.0$ μm [22]. On the other hand, the flattened dispersion range of $F_1$ and $F_2$ spans from 3.96 μm to 5.46 μm and 4.42 μm to 7.69 μm, respectively (corresponding to the dispersion $\leq 5$ ps/nm/km). These results indicate the excellent chromatic dispersion controllability of our PCF.

Figure 4 shows the chromatic dispersion [Fig. 4(a)], confinement loss [Fig. 4(b)], and nonlinear coefficient [Fig. 4(c)] of our proposed PCFs. The fibers $F_1$ and $F_2$ are pumped by lasers with 4.5 μm and 6 μm wavelengths, respectively. At the corresponding pumped wavelength, dispersion is about −2.26 ps/km/nm for $F_1$ and 4.87 ps/km/nm for $F_2$. The confinement loss and the nonlinearity profiles of the two PCFs are similar. The fibers have low loss at short wavelengths; however, the loss increases dramatically at long wavelengths due to the small diameter of the core versus wavelength range. As expected, the light field is barely supported inside the core of $F_1$ at $\lambda > 11$ μm.

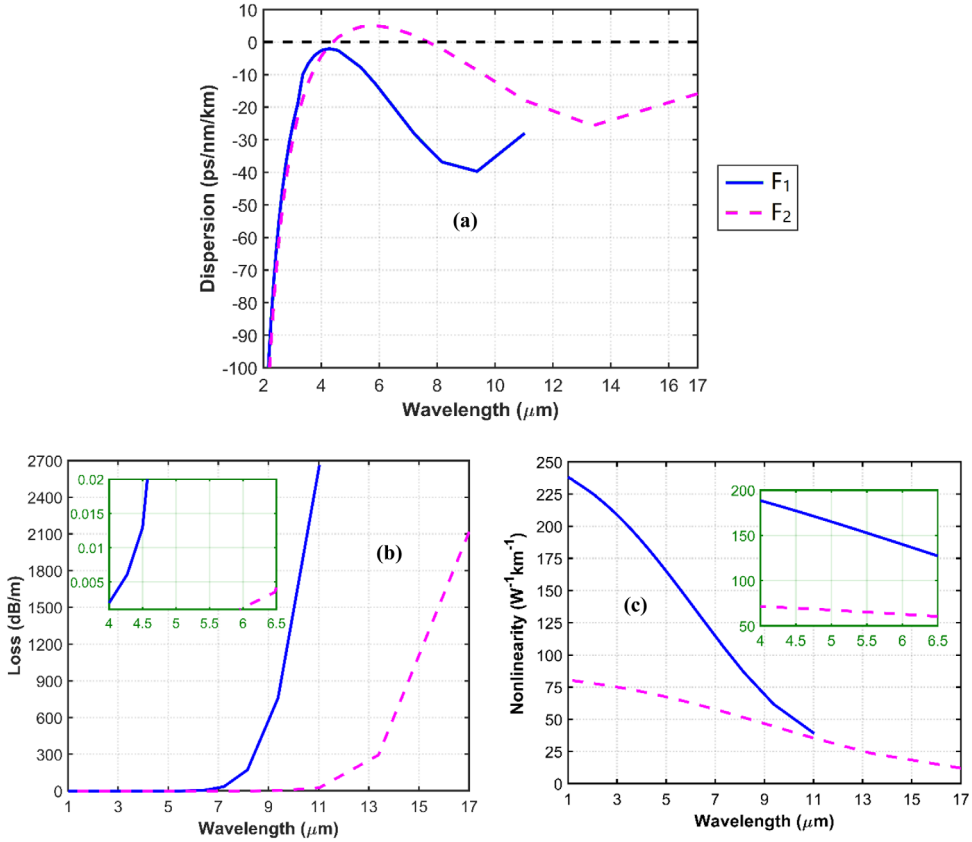


**Fig. 4.** (a) Dispersion, (b) confinement loss, and (c) nonlinearity of $F_1$ and $F_2$.

The confinement loss of two fibers is $1.29 \times 10^{-2}$ dB/m at 4.5 μm and $1.24 \times 10^{-3}$ dB/m at 6 μm, which is much smaller than reported in the publications [11,22,33–35]. The relatively large nonlinear coefficients of 177.11 $W^{-1}$ $km^{-1}$ and 69.54 $W^{-1}$ $km^{-1}$ for $F_1$ and $F_2$ are suitable for SCG.

## 3. NUMERICAL SIMULATION OF SCG IN THE $As_2S_3$ PCF WITH NEAR-ZERO FLAT DISPERSION PROFILE

The evolution of the pulse is calculated after solving the generalized nonlinear Schrödinger equation in the domain of the frequency as shown in Eq. (2), where the spectral envelope of the electric field and the distance of the light transmission are denoted $\tilde{A}(z, \omega)$ and $z$, respectively [36],

$$\frac{\partial \tilde{A}'}{\partial z} = i\bar{\gamma} \exp(-\widehat{L}z) \times F\left[\tilde{A}(z, T)\int_{-\infty}^{\infty} R(T')\left|A(z, T-T')\right|^2 \mathrm{d}T'\right]. \quad \textbf{(2)}$$

The dispersion and loss operators are defined as follows:

$$\widehat{L}(\omega) = (\beta(\omega) - \beta(\omega_0) - \beta_1(\omega_0)[\omega - \omega_0])\, i - \alpha/2, \quad \textbf{(3)}$$

where $\alpha$, $\beta$, and $\beta_1$ correspond to the total loss, the constant of the propagation, and the group velocity inverse [37]. The Raman response function including the fractional contribution of delayed Raman response $f_R$, the Dirac delta function $\delta(t)$, the Raman period $\tau_1$, damping time $\tau_2$, and Heaviside step function $\Theta(t)$ is determined in Eq. (4),

$$R(t) = \delta(t)(1 - f_R) + \frac{\left(\tau_1^2 + \tau_2^2\right) f_R}{\tau_1 \tau_2^2} \times \exp\left(\frac{-t}{\tau_2}\right) \sin\left(\frac{-t}{\tau_1}\right) \Theta(t), \quad \textbf{(4)}$$

where $f_R = 0.2$, $\tau_1 = 15.5$ fs, and $\tau_2 = 230.5$ fs are referenced in Ref. [26].

The peak power in the SCG simulation in the all-normal dispersion PCF is varied from 1 to 20 kW. The pulse duration is 110 fs, and the selected length is 10 cm.

The flattened dispersion profile of $F_1$ in the 3.96–5.46 μm wavelength range was shown in the previous section [Fig. 4(a)]. The simulation results of the output spectra of $F_1$ with various peak powers are indicated in Fig. 5(a). The SCG spectrum spans from 2.8 to 6.4 μm, more than one octave for the peak power of 1 kW. Once the pump peak power has been increased from 5 to 7 and 10 kW, an expansion of two wavelength edges to both sides could be observed. The SCG spectrum achieves more than two octaves at 15 kW, i.e., from 1.6 to 7.7 μm. The large absolute value of the chromatic dispersion and the low material transmission of $As_2S_3$ inhibit significant shifts in the short wavelength edge despite further increases in peak power [18]. However, the opposite case is observed for long wavelength edges. The higher the input power, the more they shift toward longer wavelengths.

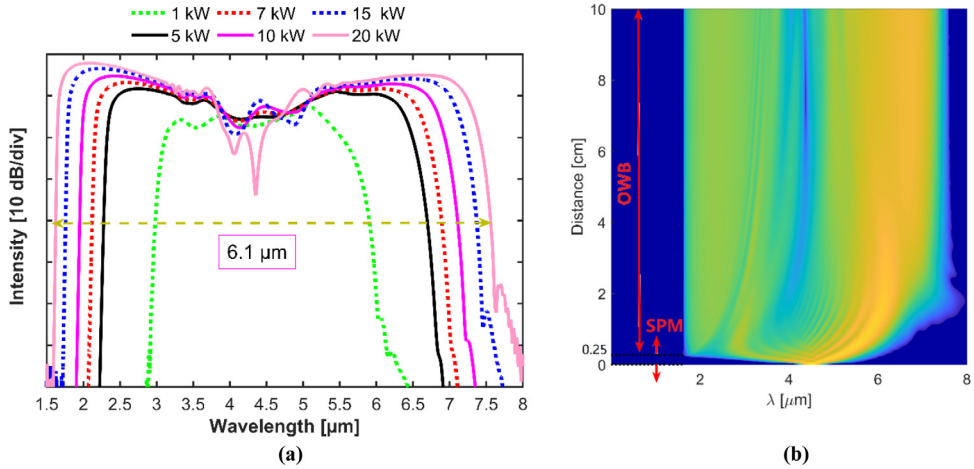


**Fig. 5.** (a) SC output spectrum along the 10 cm long fiber $F_1$ for various input power and (b) evolution of the SC at 20 kW.

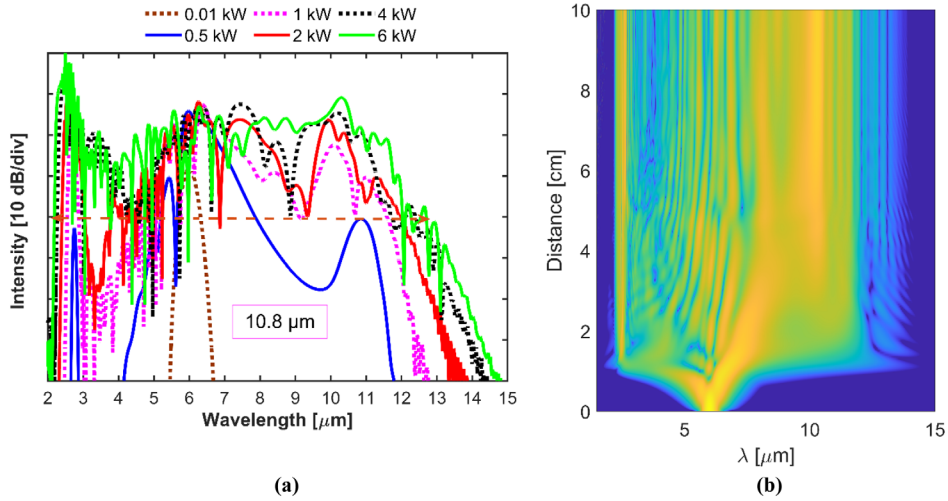


**Fig. 6.** (a) SC output spectrum along the 10 cm long fiber $F_2$ for various input power and (b) evolution of the SC at 6 kW.

It is possible to reach out to 8 μm for a long-wavelength edge as the pumped peak power is 20 kW. Consequently, the SC spectrum spans from 1.5 to 8 μm with good flatness while the bandwidth at half-maximum is 6.1 μm.

Figure 5(b) illustrates the spectrograms captured along the propagation distance $z$ within the fiber $F_1$ under a pump peak power of 20 kW. Initially, the spectrum is broadened on both sides as a result of self-phase modulation (SPM). At $z = 0.25$ cm, optical-wave breaking (OWB) happens in the short-wavelength range [38]. This phenomenon is characterized by the side lobe of the spectrum and oscillation on the trailing edge of the pulse in the time domain. The spectrum right domain records the appearance of OWB at $z = 1.25$ cm. The dominance of the main mechanisms, namely SPM and OWB, can be clearly seen in the spectral broadening of fiber $F_1$. The spectrum is then flattened to preserve pulse coherence based on energy exchange between the wavelength components.

On the basis of the above results, it can be predicted that the SCG spectrum will be broadened when pumping in the longer wavelength region. Therefore, in the next step, a 10-cm-length of $F_2$ with two ZDWs of 4.28 μm and 7.82 μm is pumped by a pulse laser with a wavelength of 6 μm and a duration of 100 fs. The soliton-driven SCG associated with the dispersive wave (DW) at the short wavelength edge results from pulse injection into an anomalous dispersion regime. At the other edge, the second ZDW is further shifted in the MIR causing the DW to disappear. At this time, the spectral broadening is directly controlled by soliton dynamics including soliton fission and soliton self-frequency shift. The pulse spectra at different powers over 10 cm of $F_2$ are illustrated in Fig. 6(a). The more the input pump power increases, the more the SCG spectrum expands. The largest spectrum roughly spans from 2 to 15 μm, and it is obtained for the pump power fixed at 6 kW with bandwidth at half-maximum of 10.8 μm. It is noticeable that the reason for the pulse splitting and periodic evolution perturbation of higher-order solitons is stimulated Raman scattering and higher-order dispersion. Therefore, after the spectrum is broadened by the SPM at the beginning of the propagation process, the pump pulse begins to transform into higher-order solitons when crossing $ZDW_1$. Once the spectrum has passed $ZDW_2$, a continuous shift to longer wavelengths is observed for each soliton before emitting DWs under the turbulence

**Table 2. Bandwidth of SC in Our $As_2S_3$ PCFs Compared with Other Chalcogenide Glass Fiber Structures**

| Refs. | Publication Year | Regime | Wavelength (μm) | Peak Power (kW) | Spectral Range (μm) | SC Bandwidth (μm) |
|---|---|---|---|---|---|---|
| [38] | 2016 | All-normal | 2.5 | 28.16 | 1–5 | 4.0 |
| [42] | 2019 | All-normal | 3.0 | 20 | 1.67–6.2 | 4.53 |
| [43] | 2020 | All-normal | 4.2 | 380 | 1.7–4.8 | 3.1 |
| [45] | 2021 | All-normal | 4.0 | 16.5 | 2.6–6 | 3.4 |
| **This work, $F_1$** | - | **All-normal** | **4.5** | **20** | **1.5–8** | **6.5** |
| [39] | 2016 | Anomalous | 6 | 750 | 1.8–14 | 12.2 |
| [40] | 2016 | Anomalous | 9.8 | 2890 | 2–15.1 | 13.1 |
| [30] | 2018 | Anomalous | 3.0 | 200 | 1.6–4.8 | 3.2 |
| [41] | 2018 | Anomalous | 2.5 | 20 | 1–10 | 9.0 |
| [44] | 2020 | Anomalous | 2.45 | 15 | 1.4–4.2 | 2.8 |
| [22] | 2022 | Anomalous | 3.5 | 7.5 | 2–10 | 8.0 |
| [46] | 2024 | Anomalous | 3.1 | 1 | 2.2–5 | 2.8 |
| [47] | 2024 | Anomalous | 6.5 | 5.83 | 2–11.5 | 9.5 |
| **This work, $F_2$** | - | **Anomalous** | **6** | **6** | **2–15** | **13** |

of high-order dispersion. Spectral bandwidth can be further expanded through additional effects such as four-wave mixing and cross-phase modulation. However, compared to the case of $F_1$, the spectral profile of fiber $F_2$ is much more complex as can be seen in Fig. 6(b). This demonstrates that the coherence is significantly reduced for soliton-induced SCG [22].

Table 2 demonstrates that our PCFs not only outperform fibers made of other chalcogenides in terms of SC bandwidth but also remarkably decrease the power used. With negligible peak power difference, $F_1$ fiber can generate a spectral range twice as broad as that in the work [45]. In addition, it is possible to reduce the input power of $F_2$ by almost five hundred times compared to the publication [40] but still obtain an equivalent spectrum bandwidth in the anomalous dispersion regime. There is no doubt that the proposed designs are expected to be popular for mid-IR SC sources.

## 4. CONCLUSION

A large-core PCF using a chalcogenide glass–$As_2S_3$ is reported in this research. The first optimized PCF $F_1$ has a flat all-normal dispersion curve from 3.96 to 5.46 μm. Its maximum dispersion is $-2.01 \pm 0.5$ ps/nm/km. Meanwhile, the $F_2$ has anomalous dispersion with two ZDWs with a flat range of 4.42–7.69 μm. Broad MIR SCG in the proposed fibers has been analyzed with different input powers. The generated SC in the proposed PCFs is among the widest SC with improved flatness when the fibers are pumped at 4.5 μm and 6 μm in the normal and anomalous dispersion regimes. Although the output bandwidth of SC is smaller with higher input powers than that of $F_2$, $F_1$ fiber possesses a flatter and smoother spectral profile, which is suitable for applications with high pulse-to-pulse coherence. Otherwise, with a SC range of 2 to 15 μm, $F_2$ can be effectively used for applications demanding broad spectral bandwidth.

**Funding.** Vietnam National Foundation for Science and Technology Development (NAFOSTED) (103.03-2023.01).

**Disclosures.** The authors declare no conflicts of interest.

**Data availability.** No data were used for the research described in the article.

## REFERENCES

1. K. Isensee, N. Kröger-Lui, and W. Petrich, "Biomedical applications of mid-infrared quantum cascade lasers-a review," Analyst **143**, 5888–5911 (2018).
2. Z. Wang, B. Zhang, J. Liu, *et al.*, "Recent developments in mid-infrared fiber lasers: status and challenges," Opt. Laser Technol. **132**, 106497 (2020).
3. E. A. Anashkina, V. S. Shiryaev, G. E. Snopatin, *et al.*, "On the possibility of mid-IR supercontinuum generation in As-Se-Te/As-S core/clad fibers with all-fiber femtosecond pump source," J. Non-Cryst. Solids **480**, 38–42 (2018).
4. N. T. Thuy, H. T. Duc, L. T. B. Tran, *et al.*, "Optimization of optical properties of toluene-core photonic crystal fibers with circle lattice for supercontinuum generation," J. Opt. **51**, 678688 (2022).
5. D. Stachowiak, "High-power passive fiber components for all-fiber lasers and amplifiers application-design and fabrication," Photonics **5**, 38 (2018).
6. X. Chen, T. Yao, L. Huang, *et al.*, "Functional fibers and functional fiber-based components for high-power lasers," Adv. Fiber Mater. **5**, 59–106 (2023).
7. M. Y. Koptev, A. E. Zaprialov, A. F. Kosolapov, *et al.*, "Visible to mid-IR supercontinuum generation in cascaded PCF-germanate fiber using femtosecond Yb-fiber pump," Fibers **11**, 72 (2023).
8. C. S. Brès, A. D. Torre, D. Grassani, *et al.*, "Supercontinuum in integrated photonics: generation, applications, challenges, and perspectives," Nanophotonics **12**, 1199–1244 (2023).
9. X. Su, R. Zhu, B. Wang, *et al.*, "Generation of 8–20 μm mid-infrared ultrashort femtosecond laser pulses via difference frequency generation," Photonics **9**, 372 (2022).
10. H. Liang, P. Krogen, R. Grynko, *et al.*, "Three-octave-spanning supercontinuum generation and sub-two-cycle self-compression of mid-infrared filaments in dielectrics," Opt. Lett. **40**, 1069–1072 (2015).
11. C. V. Lanh, D. X. Khoa, L. C. Trung, *et al.*, "Supercontinuum generation in chalcogenide photonic crystal fiber infiltrated with liquid," Opt. Mater. **137**, 113547 (2023).
12. L. T. B. Tran, N. T. Thuy, V. T. M. Ngoc, *et al.*, "Analysis of dispersion characteristics of solid-core PCFs with different types of lattice in the claddings, infiltrated with ethanol," Photon. Lett. Pol. **12**, 106–108 (2020).
13. M. Chemnitz, S. Junaid, and M. A. Schmidt, "Liquid-core optical fibers—a dynamic platform for nonlinear photonics," Laser Photon. Rev. **17**, 2300126 (2023).
14. M. M. Hasan, T. Pandey, and M. Ahasan Habib, "Highly sensitive hollow-core fiber for spectroscopic sensing applications," Sens. Bio-Sens. Res. **34**, 100456 (2021).
15. S. Hossain, M. A. Mollah, M. K. Hosain, *et al.*, "Designing of hollow core grapefruit fiber using cyclo olefin polymer for the detection

of fuel adulteration in terahertz region," Polymers (Basel) **15**, 151 (2022).
16. Y. K. A. Alrayk, B. M. Younis, W. S. El-Deeb, *et al.*, "THz dual-core liquid photonic crystal fiber with high negative dispersion," Opt. Quantum Electron. **55**, 1180 (2023).
17. S. Jiang, F. Chen, Y. Zhao, *et al.*, "Broadband all-fiber optical phase modulator based on photo-thermal effect in a gas-filled hollow-core fiber," Opto-Electron. Adv. **6**, 220085 (2023).
18. N. P. T. Hoa, T. H. Tong, L. Xing, *et al.*, "Supercontinuum generation in a chalcogenide all-solid hybrid microstructured optical fiber," Opt. Express **28**, 17539–17555 (2020).
19. N. Zhang, X. Peng, Y. Wang, *et al.*, "Ultrabroadband and coherent mid-infrared supercontinuum generation in Te-based chalcogenide tapered fiber with all-normal dispersion," Opt. Express **27**, 10311–10319 (2019).
20. C. R. Petersen, R. D. Engelsholm, C. Markos, *et al.*, "Increased mid-infrared supercontinuum bandwidth and average power by tapering large-mode-area chalcogenide photonic crystal fibers," Opt. Express **25**, 15336–15348 (2017).
21. Z. Wu, Y. Xu, D. Qi, *et al.*, "Progress in preparation and applications of Te-As-Se chalcogenide glasses and fibers," Infrared Phys. Technol. **102**, 102981 (2019).
22. C. V. Lanh, N. T. Thuy, L. T. B. Tran, *et al.*, "Multi-octave supercontinuum generation in $As_2Se_3$ chalcogenide photonic crystal fiber," Photon. Nanostr. Fundam. Appl. **48**, 100986 (2022).
23. S. Xie, F. Tani, J. C. Travers, *et al.*, "$As_2S_3$-silica double-nanospike waveguide for mid-infrared supercontinuum generation," Opt. Lett. **39**, 5216–5219 (2014).
24. S. Xie, N. Tolstik, J. C. Travers, *et al.*, "Coherent octave-spanning mid-infrared supercontinuum generated in $As_2S_3$-silica double-nanospike waveguide pumped by femtosecond Cr:ZnS laser," Opt. Lett. **24**, 12406–12413 (2016).
25. A. K. M. S. J. Choyon and R. Chowdhury, "Multifunctional chalcogenide ($As_2S_3$, $As_2Se_3$) dual-core photonic crystal fiber with elliptical air-hole for mid-IR optical communications: design and analysis," Optik **258**, 168857 (2022).
26. N. Chen, X. Zhang, X. Lu, *et al.*, "Numerical investigation of a short polarization beam splitter based on dual-core photonic crystal fiber with $As_2S_3$ layer," Micromachines **11**, 706 (2020).
27. T. Peng, T. Xu, and X. Wang, "Simulation study on dispersion properties of $As_2S_3$ three-bridge suspended-core fiber," IEEE Access **5**, 17240–17245 (2017).
28. F. Théberge, P. Mathieu, N. Thiré, *et al.*, "Mid-infrared nonlinear absorption in $As_2S_3$ chalcogenide glass," Opt. Express **24**, 24600–24610 (2016).
29. P. S. Maji and P. R. Chaudhuri, "Studies of the modal properties of circularly photonic crystal fiber (C-PCF) for high power applications," Photon. Nanostr. Fundam. Appl. **19**, 12–23 (2016).
30. N. Si, L. Sun, Z. Zhao, *et al.*, "Supercontinuum generation and analysis in extruded suspended-core $As_2S_3$ chalcogenide fibers," Appl. Phys. A **124**, 171 (2018).
31. D. V. Trong, L. T. B. Tran, H. T. A. Thu, *et al.*, "Study on dispersion characteristics of square solidcore photonic crystal fibers with $As_2S_3$ substrate," Vinh Uni. J. Science **51**, 44 (2022).
32. H. T. Duc, L. T. B. Tran, V. D. Long, *et al.*, "Optimization of the optical properties of circular lattice $As_2Se_3$ photonic crystal fibers over a wide range of wavelengths," Sci. Technol. Dev. J. **25**, 2581–2593 (2022).
33. N. T. Thuy, H. T. Duc, and C. V. Lanh, "Broadband supercontinuum generation in different lattices of $As_2S_3$-photonic crystal fibers with all-normal dispersion and low peak power," Opt. Quantum Electron. **56**, 367 (2024).
34. N. T. Thuy, "Optimization of dispersions in $GeO_2$-doped photonic crystal fibers with square lattice," VNU J. Science: Math. Phys. **39**, 56–65 (2023).
35. V. Hitaishi and N. Ashok, "Broadband supercontinuum generation using dispersion engineered $As_2Se_3$-GeAsSe-GeAsS waveguide at 6 μm," IEEE Access **11**, 12294–12302 (2023).
36. T. Cheng, H. Kawashima, X. Xue, *et al.*, "Fabrication of a chalcogenide-tellurite hybrid microstructured optical fiber for flattened and broadband supercontinuum generation," J. Lightwave Technol. **33**, 333–338 (2015).
37. B. W. Plansinis, W. R. Donaldson, and G. P. Agrawal, "Spectral splitting of optical pulses inside a dispersive medium at a temporal boundary," IEEE J. Quantum Electron. **52**, 6100708 (2016).
38. A. B. Salem, M. Diouf, R. Cherif, *et al.*, "Ultraflat-top midinfrared coherent broadband supercontinuum using all normal $As_2S_5$-borosilicate hybrid photonic crystal fiber," Opt. Eng. **55**, 066109 (2016).
39. H. Ou, S. Dai, P. Zhang, *et al.*, "Ultrabroad supercontinuum generated from a highly nonlinear Ge–Sb–Se fiber," Opt. Lett. **41**, 3201–3204 (2016).
40. T. Cheng, K. Nagasaka, T. H. Tuan, *et al.*, "Mid-infrared supercontinuum generation spanning 2.0 to 15.1 μm in a chalcogenide step-index fiber," Opt. Lett. **41**, 2117–2120 (2016).
41. M. Kalantari, A. Karimkhani, and H. Saghaei, "Ultra-wide mid-IR supercontinuum generation in $As_2S_3$ photonic crystal fiber by rods filling technique," Optik **158**, 142–151 (2018).
42. A. Medjouri and D. Abed, "Mid-infrared broadband ultraflat-top supercontinuum generation in dispersion engineered Ge-Sb-Se chalcogenide photonic crystal fiber," Opt. Mater. **97**, 109391 (2019).
43. Z. Eslami, P. Ryczkowski, L. Salmela, *et al.*, "Low-noise octave-spanning mid-infrared supercontinuum generation in a multimode chalcogenide fiber," Opt. Lett. **45**, 3103–3106 (2020).
44. S. O. Leonov, Y. Wang, V. S. Shiryaev, *et al.*, "Coherent mid-infrared supercontinuum generation in tapered suspended-core $As_{39}Se_{61}$ fibers pumped by a few-optical-cycle Cr:ZnSe laser," Opt. Lett. **45**, 1346–1349 (2020).
45. M. Meneghetti, X. Forestier, C. R. Petersen, *et al.*, "Graded index chalcogenide fibers with nanostructured core," Adv. Photon. Res. **2**, 2000091 (2021).
46. M. Sheikhmolaee, M. R. Alizadeh, S. Olyaee, *et al.*, "Supercontinuum generation in tapered planar rib waveguide based on GAP-Se hybrid chalcogenide," Opt. Quantum Electron. **56**, 4 (2024).
47. L. T. B. Tran and C. V. Lanh, "Flattened and broadband mid-infrared supercontinuum generation in $As_2S_3$ photonic crystal fibers with a square air-hole lattice," Indian J. Phys. (2024).